The GlueX Central Drift Chamber

GlueX-doc-990 (version 2)

Curtis A. Meyer
Yves Van Haarlem Carnegie Mellon University

26 February 2008

1 Introduction

Charged particle tracking in the GlueX detector is covered by two tracking systems. A cylindrical geometry around the liquid hydrogen target and a planar array in the down-stream, or forward part of the detector. This document details the cylindrical system, the Central Drift Chamber (CDC). Both tracking systems are shown in the drawing of the GlueX detector in Figure 1.

Figure 1: A cut-away view of the GlueX detector. The Central Drift Chamber (CDC) is shown as the cylindrical chamber around the target. The Forward Drift Chamber packages are shown down stream of the CDC.

The CDC will be a $1.5\,m$ long straw-tube chamber that sits at the upstream end of the GlueX solenoid and surrounds the liquid hydrogen target. It will consist of 24 layers of $1.6\,cm$ diameter straws which run from an inner radius of about $10\,cm$ to about $54\,cm$. The chamber will see charged particles coming from the GlueX target with polar angles between about 6° and 165°. It will have optimal coverage from about 16° to 150° (we define optimal coverage as crossing at least 10 layers in the chamber). Tracks going more forward than about 25° will also be seen by the Forward Drift Chamber (FDC) systems. Such tracks will need to travel through the downstream end plates of the CDC, so minimizing the material in this plates is extremely desirable.

The use of a straw-tube chamber in the central region allows us to accomplish the material goal as the straws can easily support the $\sim 50\,g$ of tension on each of the ≈ 3100 anode wires in the chamber. If one were to go with a wire-cage geometry using field wires, one would need to support about $3000\,kg$ of tension between the the end plates. Something which would require both thick end plates as well as thick shell material at both the inner and outer radius of the chamber.

In addition to minimizing material, the straw-tube designs also allows for an extremely well defined electric field through which the ionization drifts. This is especially important given the $2.24\,T$ magnetic field. With straw-tubes, the time-to-radius relation can be quite accurately computed using programs such as GARFIELD, and is extremely simple to implement in reconstruction. It also minimizes dead areas in the electric fields which are extremely difficult to model and lead to very poor position resolution for tracks passing near such regions—a situation which is almost impossible to avoid with wire-cage arrangements.

In order to achieve the physics goals of GlueX, the CDC needs to be able to measure perpendicular distances from the wires ($\sigma_{r\phi}$) to an accuracy of $\approx 150\,\mu m$. It also needs to be able to make some measurements along the length of the wire (σ_z) to an accuracy of about $2\,mm$ and be able to make dE/dx measurements that will allow us to separate kaons and pions below $450\,Mev/c$ [1]. The $\sigma_{r\phi}$ can be obtained in the straw tube arrangement. The σ_z will be achieved by placing about $\frac{1}{3}$ of the straw tubes at stereo angles of $\pm 6^\circ$ relative to the straight wires. The dE/dx will be achieved by reading out the tubes using Flash ADCs (FADCs) and then accounting for the path length in the straw.

1.1 Changes to the CDC during the last twelve months

During the last twelve months, a semi-global optimization of the GlueX detector has been carried out. One crucial goal was to minimize the material in the tracking region. However, as the process evolved, problems with shadowing of the calorimeters by chamber support structures also became apparent. The result of this optimization are changes reflected throughout the GlueX detector. Here we specifically list the ones made for the CDC.

- The length of the active volume of the CDC has been shortened from $175\,cm$ to $150\,cm$. This change is a result of the most down-stream FDC element shadowing the edges of the gap between the calorimeter systems. To alleviate this, all FDC packages were moved upstream by roughly 25 *cm* to maintain the total length between the two most extreme packages. The space for this has been obtained by shortening the CDC.

- The number of layers in the CDC has decreased from 25 to 24. This is also related to the shadowing of the calorimeter. This change allows us to bring the FDC cables out from the upstream end of the magnet, rather than through the gap between the calorimeters.
- The number of channels in the CDC has decreased from 3337 to 3098. This is a result of both the lost layer and the shortening of the chamber. The latter affects the number of tubes in a stereo layer.
- The down-stream end plate was changed from 6 *mm* Aluminum to 6 *mm* carbon fiber. This change is an attempt to reduce the material in the end-plate. However, it should be noted that much of the end plate material is actually the structures which hold the tubes and wires in place.

The following descriptions reflect the above changes to the chamber and are reflected in the current set of drawings for the CDC.

2 The CDC Geometry

The GlueX CDC is shown schematically in Figure 2. The active region is 150 *cm* long with a 0.6 *cm* thick Carbon Fiber down-stream end plate and a 0.9 *cm* thick Aluminum up-stream end plate. At the down-stream end is a 5 *cm* thick Plexiglas gas plenum which collects the gas from the straw tubes while at the upstream end is a 15 *cm* thick plenum for distributing gas to the straw tubes. An additional 20 *cm* of space for electronics is shown at the upstream end of the chamber from which all cables will be taken off the chamber. The inner and outer radius of the end plates are 9 *cm* and 57 *cm* respectively.

Radially, the chamber will consist of 24 layers of straw tubes arranged in rings around the beam line. The straw tubes are 0.8 *cm* radius aluminized Kapton tubes which surround a 20 μm diameter gold-plated Tungsten wire. Eight of the layers are placed at stereo angles of $\pm 6^\circ$. In table 1 are given the number of straw tubes in each of the 24 layers. We also give the radius of each wire at the center of the chamber and at the inside face of the two end plates. Note that for the stereo layers, the radius at the center of the chamber and that at the end plates are different. This creates dead space in the chamber volume.

Layer	Channels	Radius (cm) (center)	Radius (cm) (end plate)	Stereo (radians)
1	43	10.984	10.984	0.000
2	50	12.769	12.769	0.000
3	57	14.555	14.555	0.000
4	64	16.340	18.142	0.105
5	71	18.126	19.765	0.105
6	78	19.912	21.415	−0.105
7	85	21.698	23.085	−0.105
8	98	25.015	25.015	0.000
9	105	26.801	26.801	0.000
10	112	28.588	28.588	0.000
11	119	30.374	30.374	0.000
12	126	32.160	32.160	0.000
13	133	33.947	34.849	0.105
14	140	35.733	36.592	0.105
15	147	37.519	38.338	−0.105
16	154	39.306	40.088	−0.105
17	165	42.113	42.113	0.000
18	172	43.899	43.899	0.000
19	179	45.686	45.686	0.000
20	186	47.472	47.472	0.000
21	193	49.258	49.258	0.000
22	200	51.045	51.045	0.000
23	207	52.831	52.831	0.000
24	214	54.618	54.618	0.000

Table 1: This table shows the number of channels in each layer of the CDC. The radius at the center is the wire location half-way between the two end plates. The radius at the end plates is where the wire goes through the end plate. For axial layers, both radii are the same. For the stereo layers, the radius at the end plate is larger than it is at the center.

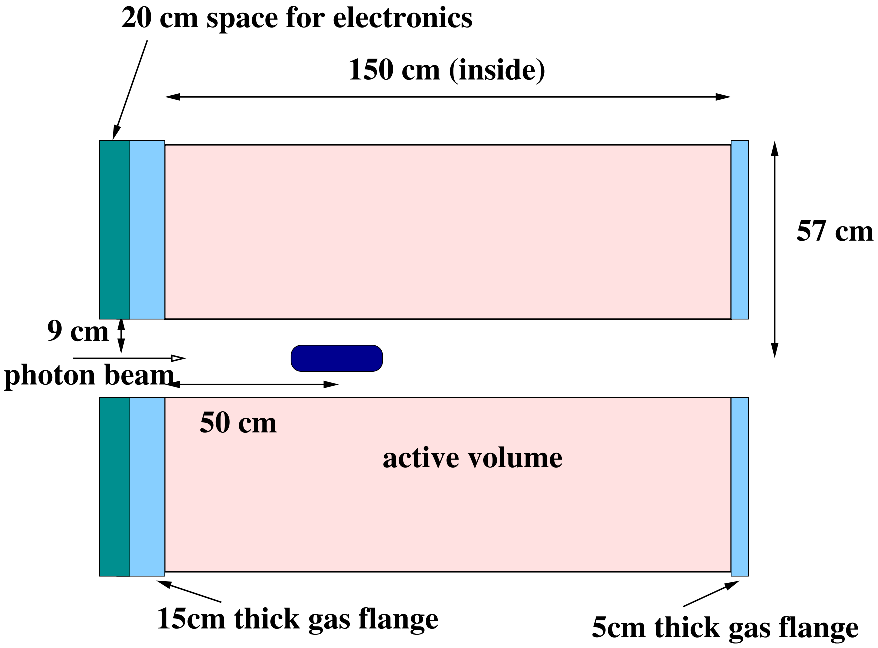

Figure 2: A side view of the CDC. The active region is $150\,cm$ long with a $0.6\,cm$ thick down-stream end plate and a $0.9\,cm$ thick up-stream end plate. At the down-stream end is a $5\,cm$ thick gas plenum which collects the gas from the tubes. At the upstream end a $15\,cm$ thick plenum for distributing gas and then an additional $20\,cm$ of space for electronics. All cables will be taken off the up-stream end of the chamber. The inner and outer radius of the end plates are $9\,cm$ and $57\,cm$ respectively.

In order to understand the the change in radius of the stereo layer, a simplified sketch is shown in Figure 3. The radius (distance from the beam line) of the wire at the end plate is given as r_e and the length of the tube is given as L. We then assume that the straw is placed with a stereo angle α. The radius of the tube at the center if the chamber is given as r_c. The fact that the radius at the center of the chamber is smaller is easily seen from the fact the the wire lies in the plane that subtends the arc along the end plate. It can be shown that

$$r_c \;=\; \sqrt{r_e^2 - (\frac{L}{2}\tan\alpha)^2}\,.$$

Similarly, if the wire is at a clocking angle of $\phi = 0$ at the center of the chamber, then the intersection of the wire with the end plates are at $\pm\phi_o$, where

$$\phi_o \;=\; \sin^{-1}\left(\frac{L\tan\alpha}{2r_e}\right) .$$

The change in radius from the center of the chamber to the end plates gets larger as the radius of the wire gets smaller. We also see that the clocking angle ϕ_o becomes larger as the radius becomes smaller.

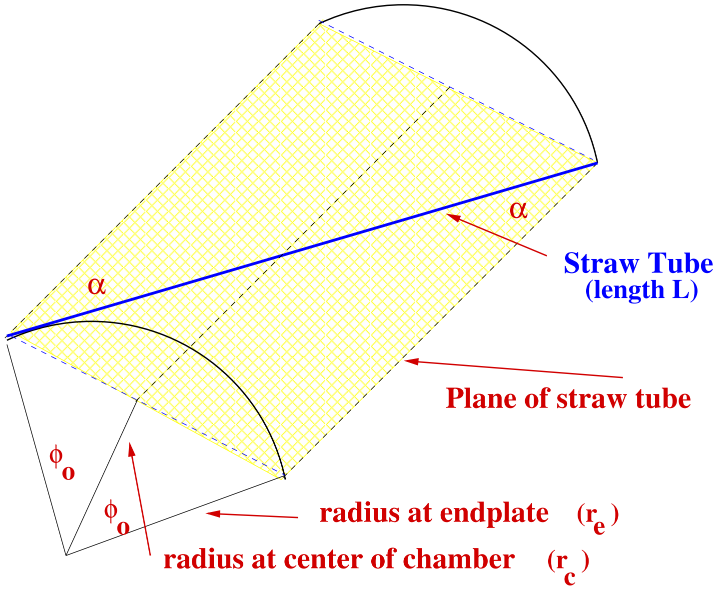

Figure 3: The placement of a stereo layer in the straw tube chamber. The radius at the center of the chamber is smaller than that at the end plates.

In Figure 4 are shown where the holes for the straw tubes will be drilled in the upstream end plate. The straight wires are shown in black, while the stereo layers are shown in color. The layout of the chamber and machining instructions are generated by a simple computer code that takes as input the inner and outer radius as well as which layers are stereo. It then lays out the chamber such that all tubes in a given layer are touching each other, and an exact integer number of tubes fit into a layer. The in-layer touching is crucial as the tubes are glued together for structural strength and the integer number eliminates dead spaces as one goes around the beam line.

The wires are held in place by a metallic crimp pin. The pin is inserted in a Delrin holder that has holes to allow gas flow. This in turn is inserted into a

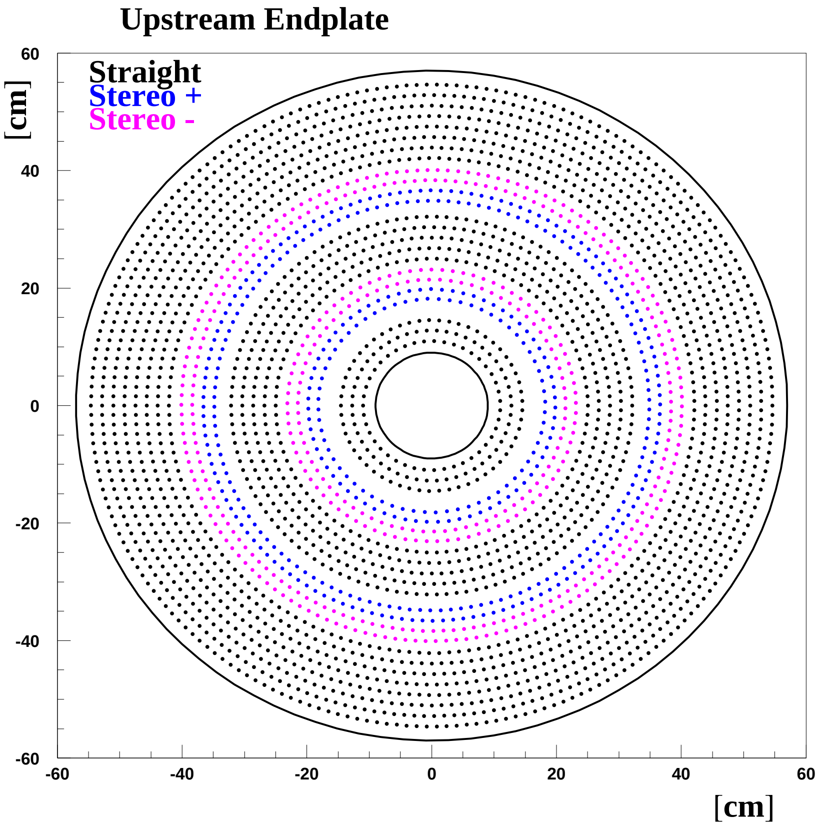

Figure 4: The drill pattern for the up-stream end plate using the 1 geometry. The black dots correspond to straight tubes. The blue dots are the +6° stereo layers while the magenta is the −6° stereo layers.

two-piece donut which is glued into the end plate. For the upstream end, the donuts are made of aluminum to provide an electrical (ground) connection between the end plate and the aluminum on the straw tube. At the downstream end, the donuts are made of Delrin to minimize the material in the chamber. Figure 5 shows schematically how the straight and stereo layers of tubes are attached to the end plates. In particular, one should note that for the stereo layers, the end plates are machined at a compound angle such that the end of the insert sits against the plate. This machining puts a minimum on the thickness of end plate.

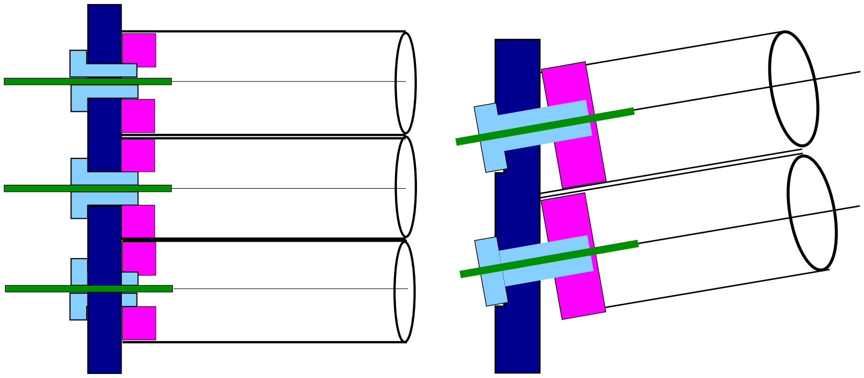

Figure 5: A schematic drawings of the feed throughs for both the normal (**left**) and stereo (**right**) wires in the CDC.

A problematic issue that is common with straw-tube chambers is the conductive glue joints that both hold the straws to the feed throughs as well as the feed throughs to the chamber end plates. Careful examination of an existing straw tube chamber from the Brookhaven EVA experiment showed that all of these joints tend to develop leaks over time. In order to try to alleviate this leak problem, a detailed study of many conducting and non-conducting epoxies was carried out to see if a good glue could be found. The conclusion of this work was that the particular choice of glue did not matter. Instead, the act of inserting one part of a feed through into another part tended to scrape much of the epoxy off the contact surface. This led to a joint with many weak spots that over a short period of time, developed leaks.

Upon careful study of this, it was decided that the only way to guarantee a good glue connection was to develop a system in which one is certain the the glue is actually making solid contact with both surfaces. The result of this is a feed through system as shown in Figure 6. The *donut* is a small tube with a small *glue trough* machined into its perimeter. From one end of the donut, a small *glue port* is drilled from the outside to the *glue trough*. Once the donut has been inserted into the straw tube, a known amount of conducting epoxy can be injected through the *glue port* into the *glue trough*. The strength of the resulting glue joint is solid, independent of the tested epoxies. In fact several test cells have maintained several psi overpressure for nearly nine months without leaking.

Into the donut, it is necessary to glue the insert that both holds the straw tube the chamber end plate and holds the crimp pin. In order to guarantee

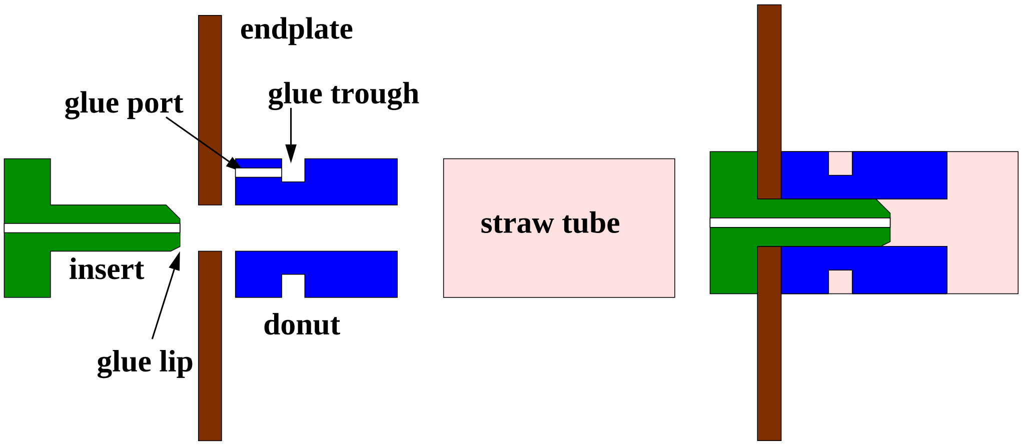

Figure 6: The CMU designed feed throughs which provide a solid glue joint between the straw-tube and the end plate. The left-hand figure shows an expanded view, while the right-hand shows the feed throughs in the chamber end plates.

a good glue joint between the donut and the insert, a small *glue lip* has been machined on the tip of the insert. If a uniform coat of glue is applied to the outside of the *insert*, then when it is inserted into the donut, the epoxy tends to collect in both the *glue lip* and between the *insert* and the chamber end plate. Exactly where we need it to guarantee a good epoxy seal. Using these specially designed feed through systems, we are able to obtain a conducting gas-tight joint with all conducting epoxies that we have tried.

These donuts that will be machined out of aluminum for the up-stream end plate and Delrin for the down-stream end plate. These parts have been manufactured at Carnegie Mellon university for the prototype chamber.

The straw tubes are clearly a crucial element of the design. Work has been done with both aluminized Mylar and aluminized Kapton tubes. It was found that the Mylar tubes were not particularly forgiving during the construction process. Any kink of bump tended to remain in the tube, thus destroying its usefulness. In contrast, the Kapton tubes tended to bounce back from just about anything. Once in place, they are much more resilient and significantly less prone to damage. The two main draw backs to Kapton are the fact that they are somewhat more expensive than Mylar, and that their *springiness* makes them more prone to gravitational sag. Gluing them securely to their neighbor tubes in the final chamber is crucial. However, based on experience with both, it has been decided that Kapton tubes will lead to a more resilient chamber, and based on the significantly lower rejection rate (5% versus 95%), will ultimately cost less than Mylar.

3 The Chamber Gas and the Gas System

The choice of chamber gas plays a significant role in the chamber's performance due to the $2.24T$ magnetic field. In order to study this, the GARFIELD program [4] has been used to compute electrostatic properties of the straw tubes, both with and without the magnetic field. The results of this work can be are summarized in GlueX note 62 [5]. Figure 7 shows an electrostatic calculation for a tube with the wire well-centered in it. Figure 8 shows GARFIELD calculations for two tracks going through a straw tube in three different gas mixtures. The three gas mixtures are Ar(30%)-C_2H_5(20%)-CO_2(50%), Ar(90%)-CO_2(10%) and Ar(50%)-C_2H_5(50%). While in all three cases the time-to-distance relationship is well defined, the longer drift distances of the spiraling tracks introduce a large diffusion contribution to the total resolution. The diffusion resolution, σ_L is also dependent on the gas. Pure argon has an extremely poor resolution, while pure carbon dioxide has a very good resolution. Finally, it is desirable to collect the electrons as quickly as possible. A slow gas, or a very long drift distance can easily push the collection time over a micro second. For this reason, the Argon-Ethane mixture shown in the lower two plots of Figure 8 is an inappropriate mixture. Investigations are ongoing to identify mixtures that will satisfy the all of the requirements. To indicate the advantage of good electrostatics, Figure 9 shows what happens to the time-to-distance relation as one goes from zero magnetic field to full magnetic field.

Currently work is being carried out using a 90% Argon, 10 % Carbon dioxide gas mixture. The gas system currently in use for the prototype will likely evolve into the final system. It consists of a electronic mixer that can handle four gas inputs with individually calibrated controls. The resulting mixture is then pushed into a mixing tank, and then delivered to the chamber. The four input gasses are filtered before entering the system. One of the gas values allows for its output to be bubbled through a chilled liquid such as water or methylal. The current design calls for several gas changes per day in the chamber with the exhaust gas being discarded. Monitors will need to be installed to monitor the temperature and the oxygen content of the input gas. In addition, a slight over-pressure system will be used to keep the gas pressure slightly above the current atmospheric pressure. Such a system will require monitoring the atmospheric pressure and ultimately correcting the chamber calibrations based on the density of the chamber gas.

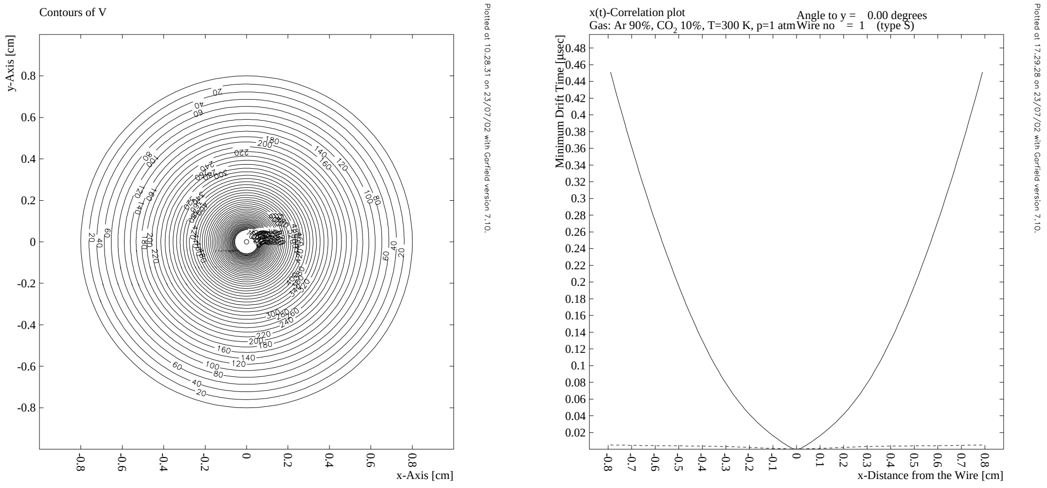

Figure 7: The left-hand plot shows a GARFIELD [4] calculation of the electric field in the straw tube. The right-hand figure shows a typical time-to-distance plot calculated for the straw-tube geometry in the $2.24\,T$ magnetic field.

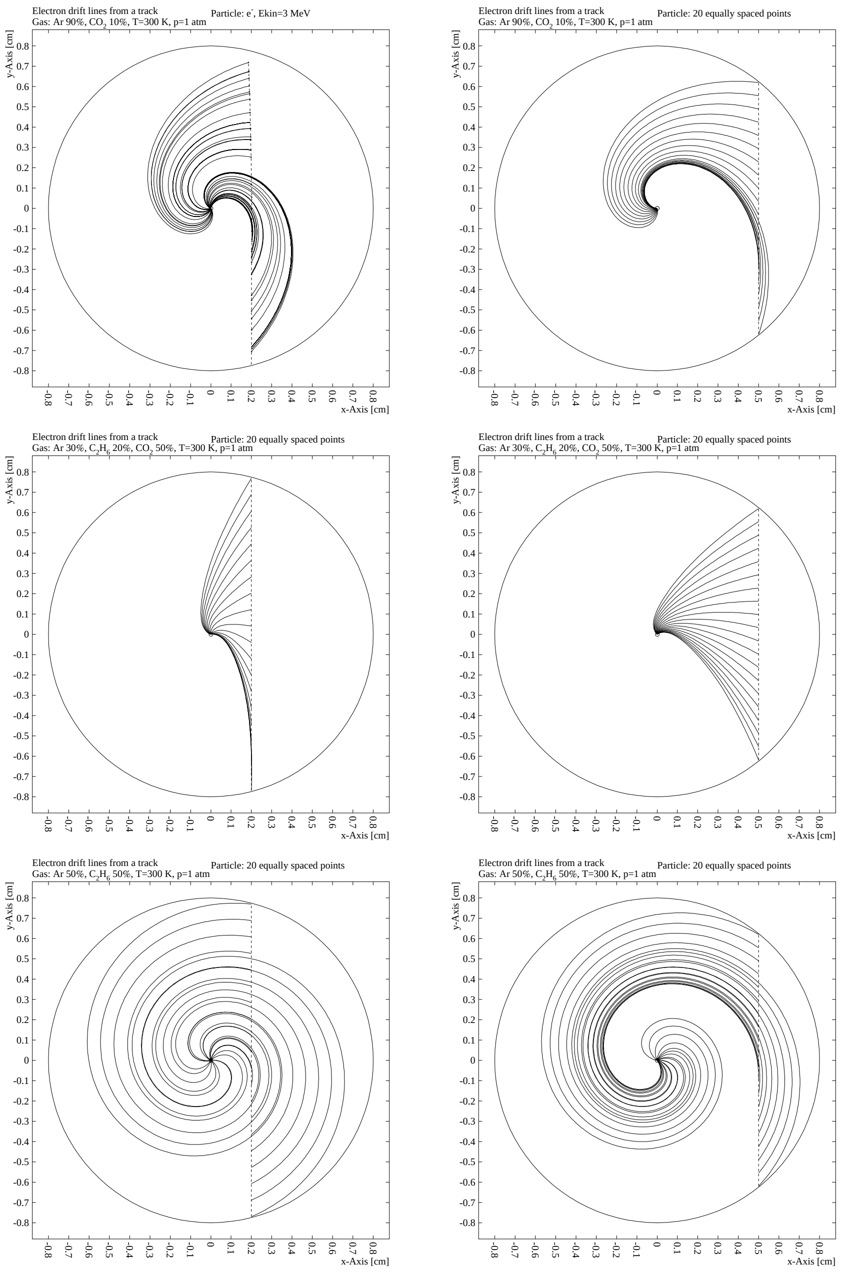

Figure 8: GARFIELD simulations of electrons drifting through a straw tube in the CDC. The curved shape of the tracks is due to the Lorentz angle induced by the $2.25\,T$ magnetic field. The upper pair are for 90/10 $Ar\,CO_2$, the middle pair are for an admixture of a hydrocarbon in the $Ar\,CO_2$ mixture, while the bottom pair are for 50/50 Argon/Ethane.

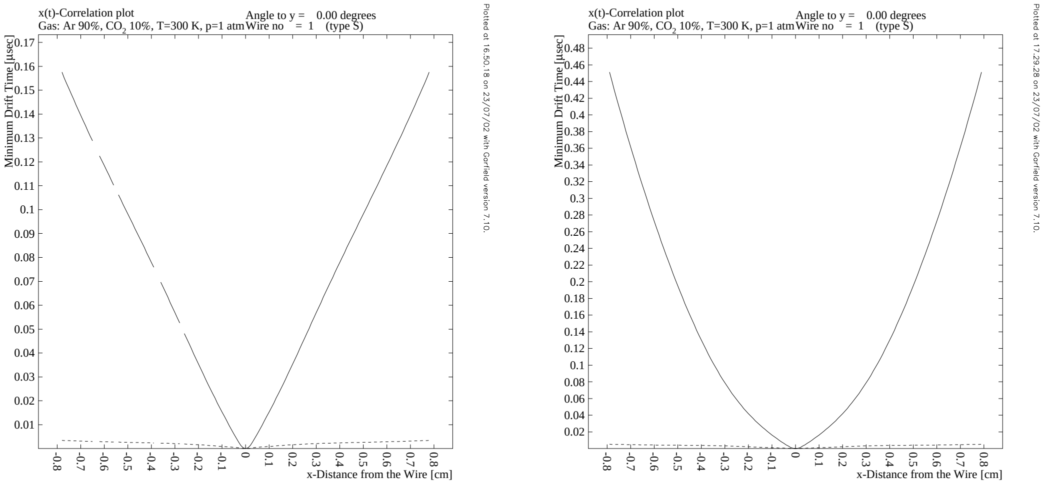

Figure 9: Calculated time versus distance in 90% Argon, 10% Carbon Dioxide mixture. **left**: No magnetic field, **right**: full magnetic field.

4 Chamber Position Resolution

In order to achieve the desired $150\,\mu m$ resolution in the CDC, we need to account for all possible contributions to the resolution. Table 2 summarizes these. Clearly the most important is the diffusion term, which depends on the gas. In order to achieve this, a gas mixture that contributes about $120\,\mu m$ for an average $5\,mm$ drift in a $\sim 2.5\,kV/cm$ electric field needs to be used. Many gas mixtures satisfy this requirement. Due to the multi-piece structure for holding the wires in place, we plan to measure the position of the crimp pin at each end of the chamber. This will let us know the position of the center of each pin to an accuracy of $40\,\mu m$. In addition to this, there is a $30\,\mu m$ uncertainty associated in the location of the wire due to the crimping of the wire. There is also a calculable gravitational sag that reaches $\approx 34\,\mu m$ at the center of the chamber, and an electrostatic distortion of about $10\,\mu m$. Both the gravitational sag and the electrostatic deflection scale with the length *$1.50\,m$) squared. The gravitational sag is given as

$$s \quad = \quad \frac{(\pi r^2)\rho L^2}{8T}$$

where the tension is measured in mass units. Typically, ρ is g/mm^3, L is the length in mm and r is the radius in mm. Data from wire vendors indicate that the yield point for tungsten wire (where is goes *plastic*) ranges from 65 to 100 grams. In ordering the wire, we will specify as large a yield point as possible, and then string the chamber at a tension of $\frac{1}{2}$ of the yield value. In the case of 65 grams, this would lead to a tension of about 33 grams and a gravitational sag of $54\,\mu m$ which would have little effect on the overall resolution of the chamber. In Table 2 we have used a $41\,\mu m$ sag corresponding to a 37 gram tension on the wire.

The timing resolution of $45\,\mu m$ assumes that the signal is digitized using $125\,MHz$ flash ADCs and that a timing algorithm that yields times to about $\frac{1}{3}$ of the digitization are used. Time fitting algorithms that are matched to the pulse shape in chambers usually yield intrinsic time resolutions around 20% of the time bin width. All of these effects are summarized in Table 2. When the effects are added in quadrature, we arrive base term due to all effects except diffusion of about $79\,\mu m$ and a diffusion term that varies from about $50\,\mu m$ near the wire to about $200\,\mu m$ for the longest drift lengths. Adding these all in quadrature yields a resolution of about 94 to $215\,\mu m$ which is well matched to the design goal of $150\,\mu m$.

Effect	Resolution μm
Diffusion σ_L	50 to 200 μm
Geometrical Precision	40 μm
Wire placement in Crimp Pin	30 μm
Gravitational Sag	41 μm
Electrostatic Deflection	10 μm
Timing Resolution	45 μm
Quadrature Total	94 to 215 μm
Design Resolution	150 μm

Table 2: The estimated contributions to the ultimate chamber resolution from various known effects. These numbers are based on 1.5 m long, 20 μm diameter, Au-W wires under 37 g tension.

The position along the length of the wire is measured using 8 layers of stereo wires tilted at $\pm 6^{|circ}$ relative to the straight layers. The nominal resolution from a stereo layer is given as

$$\sigma_z \;=\; \sigma_{r\phi}/\tan\alpha$$

where $\sigma_{r\phi}$ is the 150 μm resolution from before and α is the stereo angle. For a given crossing, we would get

$$\sigma_z \;\approx\; 1.4\,mm\,.$$

In addition to the stereo layers, it may also be possible to gang together pairs of wires at the down stream end of the chamber. There would then effectively be a readout at each end of the wire and one could use charge division to determine the position along the wire. A decision to proceed along this route will not affect the overall cost or schedule of the chamber and will e based on planned studies with the prototype. If it is possible to measure z at the $\approx 10\,cm$ level for each hit, this could greatly facilitate pattern recognition in the chamber.

5 Background Rates in the CDC

Electromagnetic interactions of the beam with the target and other material produce the dominant source of backgrounds in the GlueX detector. It is important to understand what these rates are in the CDC. This will likely limit how close the detector can be to the beam line, as well as the lifetime of the chamber. A detailed study using the Hall-D GEANT (HDGEANT) package has been carried out to calculate the rates in an individual straw tube. For purposes of the study, the tubes were placed at the positions given in Table 1. However, we also added a layer of virtual straw tubes at a radius of $6.12\,cm$ and another one at $8.15\,cm$. These added layers yield information as to how fast the background rates are rising as one moves closer to the beam line.

We note that the results reported here were carried out using $1.75\,cm$ long straws which extended $25\,cm$ farther down stream than those in the current CDC design. Since the background rates scale with the length of the straw tubes, and tend to be somewhat higher as one moves down stream, the expectation is that the rates we would see in the CDC should be slightly lower than reported here. Extensive background studies carried out to study other parts of the detector verify these assumptions—showing a rate that is about 10 to 20% lower than reported here. As such, the detailed study that originally produced these results was not repeated.

The rates were estimated by effectively counting the number of background particles over the entire length of a straw tube in each of the layers. For a primary tagged photon flux of $10^8\,\gamma/s$, the measured rates as a function of layer are shown in Figure 10.

The results for the innermost four layers (yellow in Figure 10 are summarized in Table 3. The planned CDC has its innermost straw tubes at a radius of about $10.5\,cm$, which would lead to an estimated $\approx 40\,KHz$ rate at the highest GlueX beam fluxes. While it also appears that it might be possible to move the innermost layers closer to the beam line, perhaps down to about $6\,cm$, the added material closer to the beam line is likely to degrade the performance of the rest of the detector as this would move additional material closer to the beam line. If it were desirable to make such a change, an overall optimization of the detector would need to be done with the new geometry. Such a change would also preclude the addition of a future near-target detector which might well be desirable as a future upgrade to GlueX.

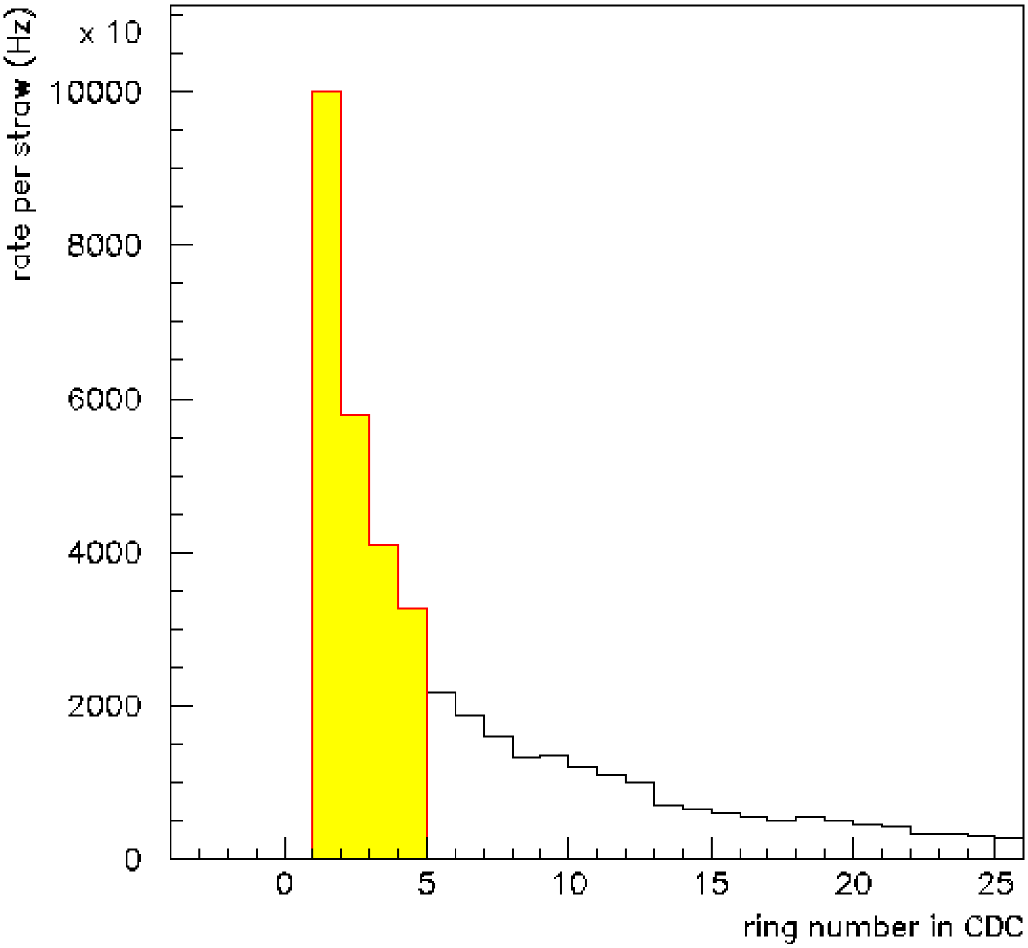

Figure 10: The electromagnetic background rates as a function of layer in the CDC for 10^8 tagged photons per second. The rates are per tube with the innermost four tubes placed at $6.12\,cm$, $8.15\,cm$, $10.19\,cm$ and $12.02\,cm$ respectively (shown in yellow in). Even at a $6\,cm$ from the target, the background rate is only $100\,KHz$ for the highest photon fluxes.

Radius	Rate
$6.12\,cm$	$100\,KHz$
$8.15\,cm$	$59\,KHz$
$10.19\,cm$	$41\,KHz$
$12.02\,cm$	$33\,KHz$

Table 3: The computed background rates for straw tubes placed at several different radiuses around the beam. The planned innermost tubes are at about $10.5\,cm$ radius.

6 Vertex Resolution

The ability to reconstruct the primary, and possible secondary vertexes is an important consideration in GlueX. The CDC is the tracking detector closest to the target, and is therefore the main component involved in vertex reconstruction. Nominally, the closer the measurements are to the beam line, the better the vertex measurement will be. The further one has to project tracks through the magnetic field, the worse things will be. Similarly, for measuring the z-coordinate of the vertex, the radius of the stereo layers in the CDC play a similar role. Simple arguments would advocate moving the first set of stereo layers as close to the beam line as possible to try and match the x-y to the z resolution. Unfortunately, for the stereo layers to provide optimal information, the tracks need to be well mapped (with straight layers) on both the inner and outer sides of the stereo layers. This leads to the configuration in Table 1 where the innermost three layers are straight.

A detailed study of the vertex resolution as a function of where the straight and stereo layers are placed was carried our and is described in GlueX note 388 [6]. The results of this study are summarized in Figure 11 where we plot the vertex resolution as a function of the radius of the innermost layer. The layer placement given in Table 1 will lead to a vertex resolution of $\sigma_{xy} \approx 0.5\,mm$ and $\sigma_z \approx 4\,mm$. It is also seen that assuming that one could move the stereo layers into $6\,cm$ would only improve σ_z to about $3\,mm$.

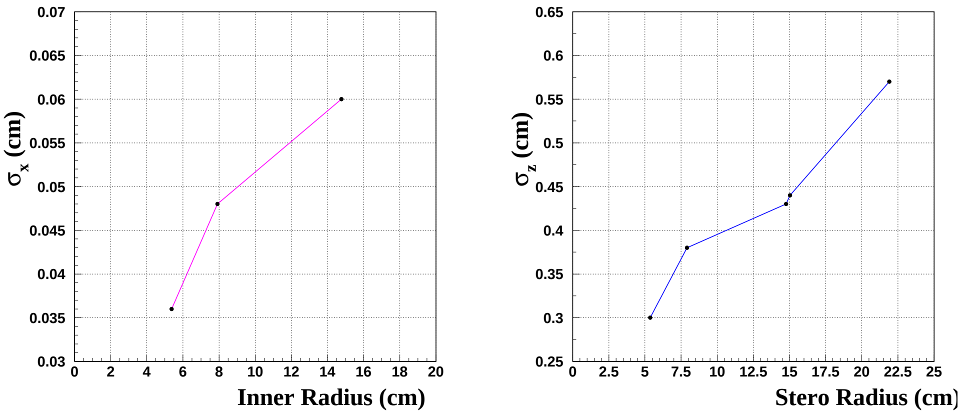

Figure 11: The estimated vertex resolution as a function of the radius of the innermost layer of tubes. For the case of the x resolution, this corresponds to the straight layers. For the z resolution, it is a function of the location of the first stereo layer.

7 Chamber Electronics

The on-chamber electronics for the CDC consist of a combination high-voltage distribution and signal translation board and the preamplifier board. Preamplifier board is common between both the CDC and FDC and is discussed elsewhere. The High-voltage board is a custom part for the CDC, but most of its individual components will be common with the FDC system. All electronics is designed to have 24 channels, so with 3098 channels, we will need 130 boards to fully instrument the chamber.

The high voltage will be provided by a commercial high-voltage system which will, through appropriate multiplexing, will provide positive high voltage to the 130 high-voltage boards, and thus to the chamber.

A straw tube chamber has the anode wires held at positive high voltage and the surface of the straw tubes held at ground. The ionization electrons produced by the passage of charged tracks through the tube drift to the anodes where they undergo gas amplification ($\approx 10^4$) and ultimately yield an electronic pulse on the wire. Because both the high voltage and the signal are on the same wire, a special high-voltage distribution board needs to be built that capacitively couples the anodes to the preamplifier. A description of this board is given in reference [12], but the relevant results are summarized here.

Nominally, the high-voltage board connects high-voltage to the wires in the CDC and couples the signals from those wires to the preamplifier cards. In doing this, there are several functions that the board performs. First, it is a low pass filter on the high-voltage input to remove ripples from the line. Second, it needs to limit sudden large currents in the case of a chamber wire breaking and shorting the high-voltage to ground. Finally, it has a high-pass filter which is used to capacitively couple the signal wires to the preamplifer cards. The design specifics of this card are similar to that for the FDC and detailed calculations can be found in the relevant FDC document [11].

The circuitry for the board is high-voltage board is shown in Figure 12. The high-voltage is supplied at the point HV, and high-frequency noise is grounded out through the low-pass filter of R_1 and C_1, while the resistor R_3 serves as protection in case of a wire breaking. The wire in the CDC is fed through the point labeled Wire. Finally, the signal from the chamber is goes through the high-pass filter of C_2 and R_2 and into the preamplifier which is mounted directly on the high-voltage board. The current design calls for all surface mount components with $R_1 = R_3 = 1\,M\Omega$, $R_3 = 100\,K\Omega$

and $C_1 = C_2 = 330\,pF$. A justification for these values can be found in references [12] and [11].

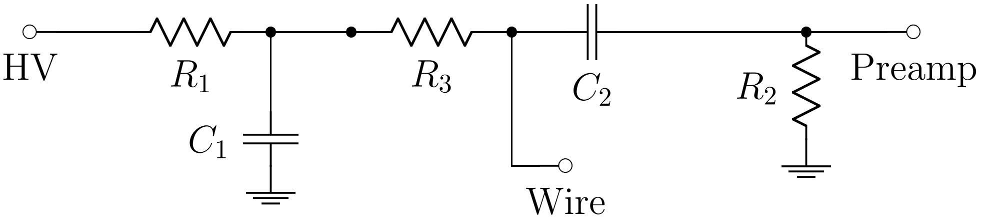

Figure 12: The CDC High-Voltage Distribution Board. In the final design, we anticipate that R_1 and R_3 are $1\,M\Omega$ while R_2 is $100\,k\Omega$. The decoupling capacitor C_2 will be $330\,pF$. The nominal design calls for C_1 and C_2 to be the same to minimize components.

The on-chamber electronics mount on the outside of the up-stream gas plenum as shown in Figure 2. The mounting is shown schematically in Figure 13. The design shown here is what is currently employed on the CDC prototype. A pair of custom 12-channel feed throughs bring allow connection between the CDC and the high-voltage board. in this design, the wires are potted in the feed throughs, soldered to the high-voltage board, then installed on the plenum and connected to the chamber wires. The connection is made by soldering a small ball of solder to the end of the cable coming through the feed through and then slipping putting this in a small tub of conducting rubber which then slides over the crimp pin on the CDC. This provides a very solid connection to the chamber and is the same procedure that was used in the CLAS region one chamber which was built at Carnegie Mellon about 12 years ago.

We are also investigating a design where a commercial connector is potted into the gas plenum and the high-voltage board plugs into it. While this looks to be a significantly better solution, we are waiting on delivery of the connectors to test this. We note that the final decision on this is cost neutral to the project. We have a solution now that will work and are pursuing improvements to this design that will simplify cabling of the chamber and long-term electronics maintenance.

The chamber preamplifier will be common with the FDC system and are currently being prototyped by members of the GlueX collaboration at the University of Pennsylvania. The final preamplifier will mount directly on the high-voltage board and then drive a 24-pair cable that will connect into to

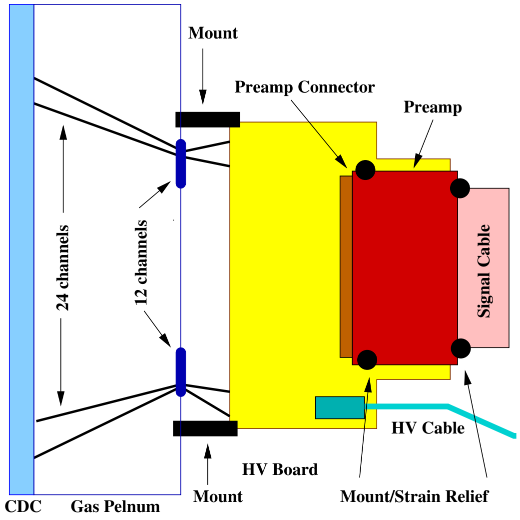

Figure 13:

a shaper board designed by Gerard Vissar at Indiana. This will then feed into a Flash ADC (FADC) system running at a rate of at least $125\,MHz$. The same electronic chains will be used for both the CDC and the FDC. Currently, prototypes of all relevant electronics are in use on the prototype CDC. A description can be found in reference [12].

Based on our experience with other chamber systems and what we have learned about straw-tube chambers from other groups, we have always anticipated that grounding is an important issue. There are currently global plans for grounding of electronics of the drift chambers as documented in reference [13] and [14]. With regard to the chamber itself, the Aluminum on the surface of the straws is connected to the feed throughs using conducting epoxy. The feed throughs them selves are then connected to the upstream aluminum end plate with conducting epoxy. All components are cleaned before application of the epoxy and all connections are over a fairly large surface area to insure a good connection. The end plate of the chamber has a heavy grounding strap that connects to the readout electronics at the level of the high-voltage board. In work with the prototype, we have found that optimal performance is achieved when a solid ground connection between the preamplifier and the chamber is made. In addition, we have found that shielding the up-stream plenum with aluminum foil which is then connected to the heat sink of the preamplifier reduces noise in the system by about a factor of 10. This is discussed in Section 13.

8 Chamber Assembly

The assembly of the final CDC is based on experience gained in constructing a 2-meter long prototype at Carnegie Mellon University. For the CDC, most parts will be sent out to commercial vendors. Because of the stereo layers, the end plates will need to be machined on 5-axis CNC machines. During this process, fiducial marks will be placed on the end plates to allow for later alignment. The feed throughs, crimp pins, wires and straw tubes will also come from commercial vendors. As the parts arrive, they will be visually inspected and sorted into acceptable and unacceptable parts.

The stringing of the straw-tube chamber occurs in a vertical orientation. The two end plates are placed around an axial tube with support plates for both top and bottom. The tube aligns the two plates radially, but does not fix the angular orientation. This latter step is accomplished with ten support rods which connect near the outer radius of the two end plates. The alignment is achieved by plumbing the two plates relative to each other. Once the rods are secured to the plates, they remain in place.

After the two end plates have been aligned, we are ready to start installing straw tubes. Preparation of the straw tubes starts with a visual inspection to make sure that there are now defects to the straw. Then the straw is cut to the appropriate length (longer for stereo than straight layers). The cutting occurs with a high speed (10,000 rpm) saw using a very thin blade. The tubes are held in place with a round clamp just next to the point where the cut is made. After the cut is completed, an alcohol covered cotton ball is blown down the length of the tube to remove residual dirt and dust. A picture of the saw is shown in Figure 14.

At this point, donuts are glued into each end of the chamber. These donuts are designed to have a glue o-ring that is filled by forcing glue into the donut with a syringe. It is possible to visibly see when the glue has gone all the way around the tube. These tubes then cure for at least several hours before installation in the chamber. This gluing is shown in Figure 15.

Installation of the straw tubes occurs in a layer-by layer process. To facilitate this installation, a ring form is machined for each layer that accurately positions the straws at the center of the chamber. All tubes for a particular layer are glued into the end plates using the alignment form, and are

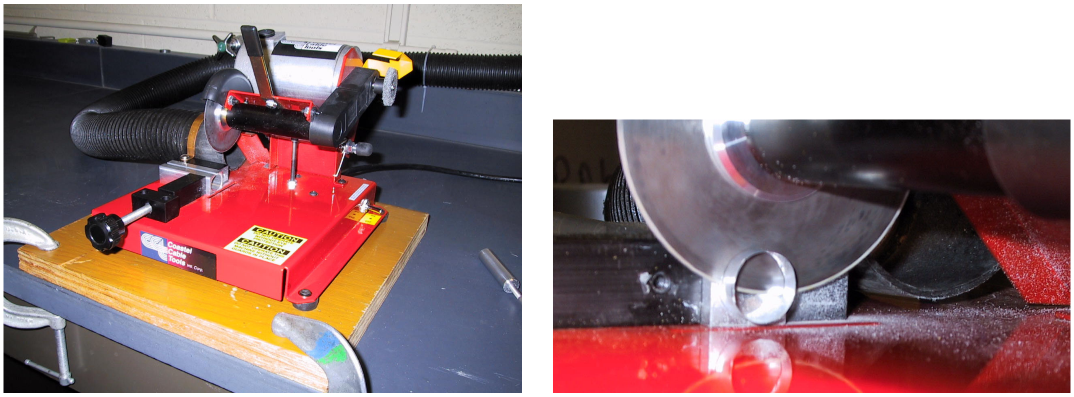

Figure 14: The high-speed saw used to cut the CDC straw tubes to the appropriate length. The black knob on the left-side of the saw tightens a clamp that holds the tubes in place for cutting. The right-hand picture shows a straw being cut by the saw.

then glued using epoxy to their neighbor tubes. Also, during installation, the tubes are spot glued to the next innermost layer. Figure 16 shows a photograph of the prototype CDC chamber hung vertically for stringing.

Once all tubes for a particular layer are installed, wires are strung in each layer. The wires are threaded through a magnetic needed which is then lowered through the tube and caught at the bottom of the chamber. The wires are then threaded through the crimp pins. The top is crimped, and then $50\,g$ of tension is applied at the bottom end of the wire, after which it is also crimped. The crimping is accomplished using a pair of pneumatic crimpers whose heads have been machined specifically for the crimp pin. To maintain consistency, then crimp is made by resting the crimping tool on the end of the plastic feed through and then crimping the wire. The crimp occurs a couple of millimeters above the plastic pin holder.

Once a layer is finished, the tension on the wires is checked using a wire tensioning device that works by placing a magnetic field near the wires, then driving the wires with an AC voltage. When the frequency of the AC voltage matches the resonance frequency of the wire, a clear resonance peak is observed. The frequency is then easily converted into actual tension using the wire length and material properties.

The procedure is then repeated for the next layer moving out until the chamber is strung. For the stereo layers, it is possible to tilt and rotate

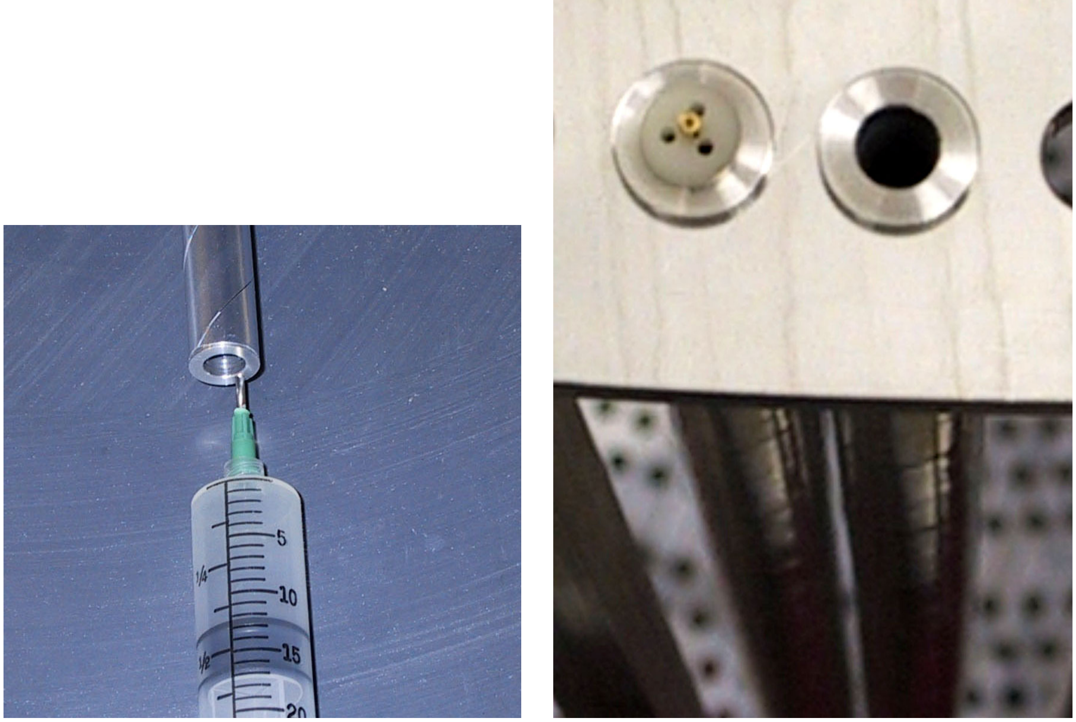

Figure 15: (left) Shows a donut being glued into a straw tube. (right) Shows the feed throughs holding a straw tube in place at the end of the chamber. Note the crimp pin in the center of the feed through and the tree holes to allow gas to flow into the straw tube.

the stringing apparatus such that the tubes and wires are installed in a vertical orientation. After all wires have been strung, spot checks will be made throughout the chamber to assure that the tension has not slipped. In addition, all wires will be electrically checked to make sure that they have not broken.

At this point, the chamber is brought to a horizontal position and the outside shell is installed. After which the support axis is removed and the inner mylar window is installed. At this point, the position of the crimp pins at each end of the chamber will be mechanically measured relative to fiducial marks on the ends of the chambers. This can be done a $40\,mum$ accuracy and alleviates the need to try and hold extremely tight tolerances on all the feed through components. There will also be an uncertainty of about $30\mu m$ associated with crimping a $20\,\mu m$ wire in a $100\,\mu m$ diameter hole.

The downstream gas plenum is installed, after which the upstream plenum is installed. Independent of which feed through scheme is used, there will be an involved process to connect wires to the crimp pins and bring them through the end plates. To minimize cabling errors, a detailed spread sheet and check-off list will be used to associate an straw tube with an electrical channel in the the readout. After all channels have been wired, a check will be made for shorted wires and bad channels will either be restrung, or disconnected.

At this point, the electronics can be connected to the chamber and high voltage can be applied to all channels. In addition, we will verify that cosmics can be seen on all channels. The chamber will then be shipped to Jefferson lab for installation in the GlueX detector.

Figure 16: The CDC prototype in its vertical position while straw tubes are installed and wires are strung.

9 Construction Schedule for the CDC

Upon completion of the final design for the GlueX CDC, the Carnegie Mellon University (CMU) group will take on the responsibility of building the final chamber for the experiment. This responsibility includes the detector itself as well as the electronics that mount directly on the detector (HVDB). The electronics chain from the preamplifiers into the Data Acquisition system will be the responsibility of other members of the GlueX collaboration.

The tasks necessary to build this chamber are shown along with a time line in Figure 17. The start date for this construction project is contingent on funding for the GlueX experiment. The tasks outlined represent approximately three years of work by the CMU group. This plot is also detailed in Table 4. With a flexible purchasing procedure, it may be possible to preorder much of the material, and shorten the project by up to one year.

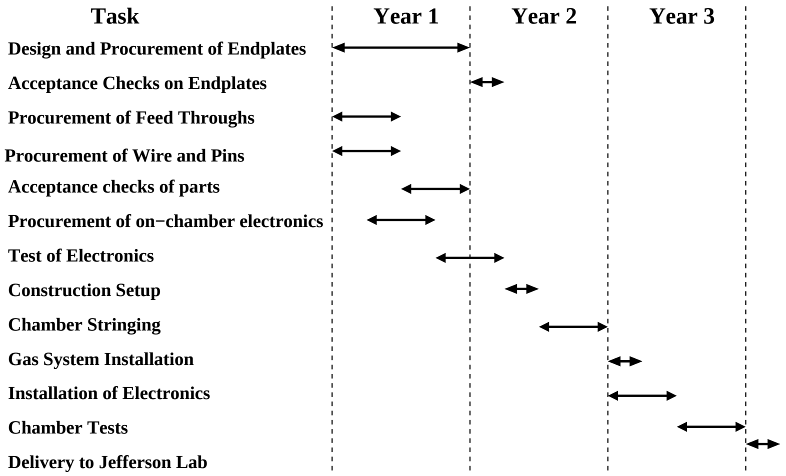

Figure 17: A time line for the construction of the CDC for the GlueX experiment. The start date and schedule are dependent on funding.

10 Chamber Installation and Calibration

The CDC will sit on a pair of rails located inside the solenoidal magnet. For installation and extraction of the chamber, the rails will *mate* with external rails mounted to a cart on the upstream side of the detector. The CDC

Timetable for R& D	
+0 to +12 months	Design and Procurement of chamber end plates.
+0 to +6 months	Procurements of feed throughs.
+0 to +6 months	Procurement of wires and crimp pins.
+3 to +9 months	Procurement of on chamber electronics
+6 to +15 months	Acceptance checks of parts.
+9 to +15 months	Tests of electronics.
+15 to +18 months	Construction Setup.
+18 to +24 months	Chamber stringing.
+24 to +27 months	Gas System Installation.
+24 to +30 months	Installation of electronics.
+30 to +36 months	Chamber tests.
+36 to +39 months	Delivery to JLab.

Table 4: The time line for construction and delivery of the final straw tube chamber for GlueX. Start time is defined as start of construction funding.

will be able to be inserted and extracted with its cabling intact. Positioning of the chamber will include fiducial marks that can be surveyed as well as possible positioning pins. The final such system still needs to be designed. However, it is crucial that the relative position of the CDC and the FDC be accurately known in order to achieve that ultimate resolution. In addition, for regions where the magnetic filed is not uniform, it will be necessary to know the absolute locations of the chambers with reasonable accuracy.

For calibration of the chambers, there will be a system that allows us to send pulses down to the inputs of the preamplifier. This will allow for a relative timing measurement of each channel as well as a method to monitor gain variation in individual channels. As noted earlier, it will also be necessary to monitor the gas pressure and temperature and then make corrections for density changes in the gas.

The starting point of the reconstruction will be a time-to-radius relation that can be accurately calculated using the GARFIELD program. With this as a starting point, we anticipate being able to select a reasonable profuse reaction that can be reconstructed and then used to fine tune the calibrations.

11 Chamber Maintenance

The CDC is designed such that all the electronics is on the up-stream end of the chamber. These will be accessible without removing the chamber from the magnet. In the case where a wire were to break and short out against the side of the straw tube, we anticipate that the High Voltage will be distributed in blocks such that some section of the chamber could be turned off. It is also possible from the upstream end to disconnect the high voltage from a single wire, though the operation of moving things out of the way may well make this one to two shift long operation.

12 Safety Considerations

The CMU group has an excellent working relationship with the CMU Environmental Health and Safety (EH& S) department. Input from EH& S is sought on all issues that could impact safety at Carnegie Mellon University. Historically having built major pieces of equipment for the past thirty years, there have been no reportable injuries over this time.

During chamber operation, the most likely safety concern is the chamber gas. At the moment, the gas mixture contains only argon and carbon dioxide and is not considered dangerous. There is some chance that the ultimate gas mixture will contain a small ($\approx 10\%$) admixture of a hydrocarbon. Appropriate controls will need to be designed into the gas system to make sure that this is handled correctly.

13 The Full-scale Prototype

Over the last several years, the Carnegie Mellon group has performed a significant amount of R&D work related to the CDC. This work included the construction of a $2\,m$ long chamber that represents $\frac{1}{4}$ of the circular end plate. As a historical note, the $2\,m$ length was the original proposal for the length of the CDC, which has since through a series of studies been reduced to the current planned $1.5\,m$ length. The prototype contains about 70 straw tubes, of which most have been strung with wires. The straws included both aluminized mylar and aluminized kapton. In addition straight and both directions of stereo layers have been installed, with particular emphasis paid to the transition from one to another. Figure 18 shows a picture of the prototype on the test bench at CMU.

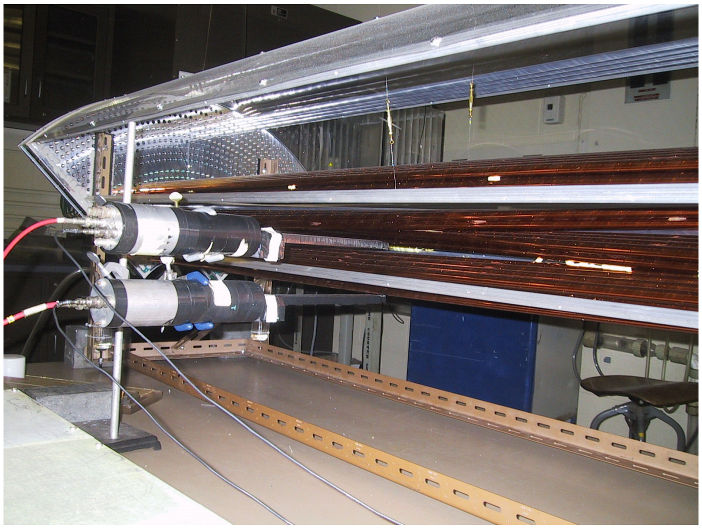

Figure 18: A photograph of the $2\,m$ long CDC prototype at Carnegie Mellon. The copper-colored tubes are kapton and the silver-colored ones are mylar. Also shown are a pair of small scintillators used in a specialized cosmic trigger.

Various material questions were addressed through the prototyping period, most of which have been summarized earlier in this report. Initially, we determined that the end plates would need to be produced as single pieces, which will require an external firm to take on the job. Test with two-piece end plates (octant) showed that we could not maintain relative position accuracy at the desired level. Tests were also made with both Mylar and Kapton tubes, with a final decision be made in favor of Kapton. This is driven by both robustness and cost. We have also manufactured samples of all of the parts that will be used in the final chamber. This includes feed throughs, gas plenums, electrical connections and high-voltage board.

The prototype chamber currently has sixteen instrumented channels (the number of FADC channels available), and is set up to collect cosmic ray events using a pair of roughly $20\,cm$ by $20\,cm$ scintillators placed above and below the chamber with about $80\,cm$ between them. The signals from the chamber go through a 2'nd generation high-voltage board that contains the capacitors that will be used in the final board. This board has 16 rather that the final 24 channels that will be used. Into the high-voltage board is plugged in a prototype ASIC preamplifier. This preamplifier board has two of the three eight-channel ASIC chips on it. We note that a final run is planned on the ASIC later in 2008 based on feed-back from both the CDC and FDC studies. The preamplifier board outputs a differential signal that goes through a $30\,m$ long, 24-channel twisted pair cable. The cable, in turn, plugs into a 24-channel receiver/shaper board that will be used for the final chamber. The output from the shaper board then goes to two 8-channel, $200\,MHz$ commercial Flash ADC board (Struck DLxxx) in a VME 64x crate. The Flash ADC's are then read out using CODA, the Jefferson Lab data acquisition system that will be used in GlueX.

13.1 Noise Reduction

Minimizing noise pickup in the CDC is crucial to enabling the best possible resolution in the final chamber. In this section we detail some of the work that has been done with the prototype and point out the important lessons that will be crucial in the final chamber construction. Most crucially, these steps involve shielding and grounding of the chamber and the electronics. We highlight this work by three pairs of plots, each of which shows a *before* on the left and an *after* on the right. The first (Figure 19) shows pulses seen on the prototype. The before plot on the left shows fairly significant noise everywhere along the pulse and also a significant *ringing* just before the physics pulse. This ringing was found to be associated with a computer monitor about two meters from the electronics. The right-hand pulse shows the substantial noise reduction achieved. On the scale shown, it is almost impossible to see the noise on the chamber.

An alternative way to look at this is to look only at the pedestal signal on a straw. Figure 20 shows a pair of scope traces for the same channel for both before and after. Both traces are on the same scales on the scope ($2\,mV$ per division). The noise is well under a mV after improvements. Finally, Figure 21 shows a plot of the data in the pedestal bins from the FADC system for both before and after. The point to note here is the relative widths of the two distributions. The before plot goes from roughly 300 up to 1500 channels, while the after goes from roughly 860 to 1060. The absolute value is not relevant, but the reduction in width is very significant.

In looking to reduce noise, a number of steps were tried. These included heavy grounding straps for the chamber end plate to various points in the electronics, wrapping the straw tube volume with grounded foil, wrapping

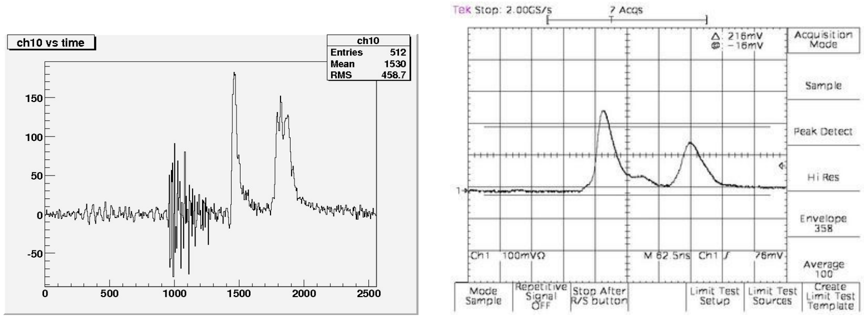

Figure 19: (left) A signal pulse as seen on a straw before work on grounding and noise reduction. (right) A signal pulse after improvements. The ringing that is a bit earlier than the pulse in the right-hand plot comes from a computer monitor in the vicinity of the chamber.

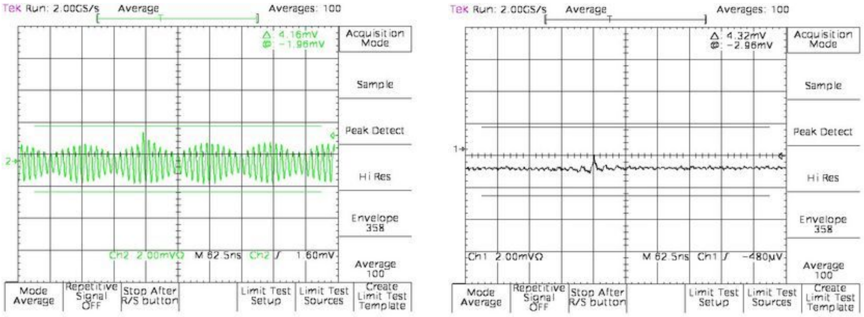

Figure 20: (left)Noise on a straw before work on grounding the prototype. (right) The noise on the same channel after the grounding. The noise has been reduced by about a factor of 10. Both plots are on a $2\,mV$ and $62.5\,\mu s$ per division scales.

the gas plenums with foil, and multiple and varied combinations of the above. In the end, the most significant reduction (nearly all the factor of 10 that was achieved) was due to wrapping the two gas plenums in grounded foil, making a single solid ground connection from the end plate to the high-voltage board, and **most crucially**, connecting the heat strap on the preamplifier board to the foil around the up-stream gas plenum.

Based on this work, we believe that a heftier ground connection between the preamplifier board and the high-voltage board is needed. This then needs to be grounded to the end plate of the chamber. It also appears quite

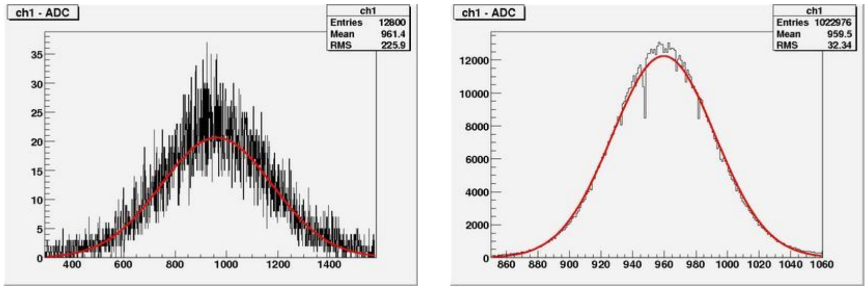

Figure 21: (left) The pedestal on a straw before work on grounding and noise reduction. (right) The pedestal on the same channel after improvements. Note that the final pedestal is significantly narrower than what it was originally.

important to have the gas plenums wrapped in shielding foil.

While we recognize that the final chamber as installed in the GlueX detector will have its own grounding issues, the lessons learned with the prototype have lead to a better grounding plan for the electronics and final chamber.

13.2 Pulse and Track Fitting

There are several methods to fit drift time using Flash ADC data. The most common is the so-called first electron method which we will describe in some detail. Alternatives include the differential center of gravity and fitting pulse shapes to the rising edge of the pulse. The first electron method fits a straight line to some part of the rising edge of the pulse and then takes the intercept of the line with the amplitude axis to be the drift time, (arrival time of the first electron). In fact, it is not the intercept with the amplitude axis, but rather when the amplitude is equal to the pedestal (the noise in the system) that is taken. The pedestal can be computed several different ways and then subtracted out from the pulse data. For the following, we will assume that we have pedestal-subtracted data.

In fitting the leading edge, there may be some choice in what part of the data to use. We show a pedestal subtracted pulse in Figure 22. The are four points on the leading edge, but a choice for fitting could be the first n, where $n = 2, 3, 4$, or we could ignore the first point and then fit the 2'nd and 3'rd, or the 2'nd, 3'rd and 4'th. Typically, one would like to ignore the first point, but it is also desirable to have more than two point to fit to. In such a scenario, one would like the leading edge of the pulse to be roughly 4 to 5 FADC channels long, which usually implies that the pulse is shaped to achieve this.

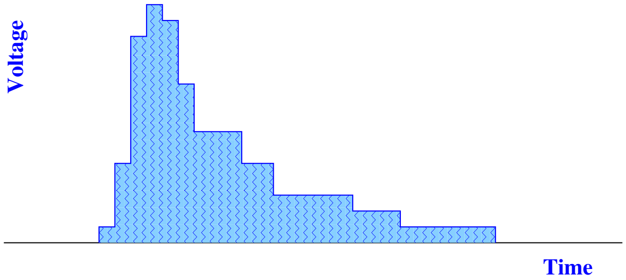

Figure 22:

In the following, we assume that we will fit the first n points of the pulse. Along the rising edge, we have several pairs of points , (y_i, t_i). These are fit to a straight line to yield a slope α and intercept y_0.

$$y = y_0 + \alpha t$$

Doing a simple least squares fit, we can solve for y_0 and α by computing a number of sums. If there are n points along the leading edge used in the fit, we find that

$$\begin{aligned} y_0 &= \frac{\sum_{i=1}^{n} y_i \sum_{i=1}^{n} t_i^2 - \sum_{i=1}^{n} t_i \sum_{i=1}^{n} y_i t_i}{n \sum_{i=1}^{n} t_i^2 - \left(\sum_{i=1}^{n} t_i\right)^2} \\ \alpha &= \frac{n \sum_{i=1}^{n} y_i t_i - \sum_{i=1}^{n} t_i \sum_{i=1}^{n} y_i}{n \sum_{i=1}^{n} t_i^2 - \left(\sum_{i=1}^{n} t_i\right)^2} . \end{aligned}$$

From these, the first-electron drift-time of the pulse is defined to be the intersection of the line with the $y = 0$ axis and can be computed from y_0 and α as follows.

$$t_e = -\frac{y_0}{\alpha}$$

For the pulse shown in Figure 22, we report the computed t_0 based on the first 2, 3 and 4 bins of the rising edge. The reported t_0 is the fraction of the way into the first bin. Over varying pulse shapes and sizes, one typically finds an uncertainty on the order of $\frac{1}{4}$ of a bin width with 3 to 4 samples on the rising edge. Table 5 shows these fits for the given pulse.

n	y_0	α	t_e
2	-0.75	5.0	0.15
3	-0.78	6.0	0.13
4	-0.26	4.9	0.05

Table 5: Fit first-electron times from the pulse shown in Figure 22.

Data from a large number of pulses are collected and the measured drift time for each channel is looked at. A fit is made to determine what the earliest time on each channel j is, t_0^j. In analyzing data, the drift time then utilizes both the t_0 and the first electron time, t_e to yield the drift time.

$$t_d^j = t_e^j - t_j^0$$

Using the resulting t_d^j, a look-up table computed using Garfield (see section 3 converts the drift time to a distance from the wire, r^j. This distance is then combined with the location of the wire (x_w^j, y_w^j) to define a *drift circle* to which the primary track is tangent. Figure 23 shows an example of a track going through four straw-tubes. The drift circles are shown around each of the four wires. A fit can be done to then define the best track parameters that reconstructs tangent to all the drift circles. Looking carefully at Figure 23, there is no other track candidate that would fit as well as the true track shown in the figure.

13.3 Chamber Resolution Studies

Resolution studies in the CDC prototype are currently being performed. Sixteen channels which span six layers in the CDC have been instrumented and are readout using the electronics described above. Cosmic events are triggered using a pair of $20\,cm$ by $20\,cm$ scintillators placed above and below the chamber. The chamber is run using a 90/10 mixture of $Ar\,CO_2$ gas with a nominal voltage of $1850\,V$ on the anode wires. Data runs go for roughly 72 hours after which sufficient statistics have been collected to look at chamber resolution.

As the trigger may change from run to run, the first step in the analysis is to determine the t_0 (see Section 13.2) for each wire. The data are then analyzed to get the drift time from each found pulse. Events with more than three straws hit can then be used for resolution studies. The most optimal

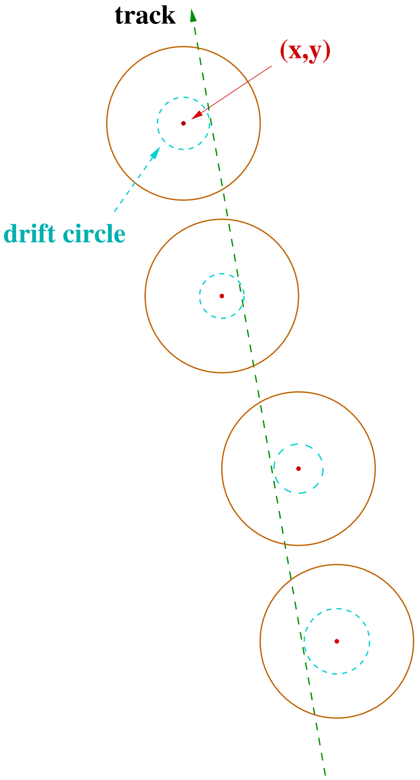

Figure 23: A track going through four straw tubes in the CDC. The straw tubes are shown as the large circles and the location of the wire is indicated as the dot at the center of the circles. The track passes through the wires and the first ionization in each tube comes from the point where the track intersects the dashed circle inside the straw tube. Fore each hit, we then have the (x, y) coordinate of the wire and the radius of the dashed circle.

events for these studies involve events which have hits in each of the six instrumented layers, but given the low rate of cosmics, and the relatively large size of the paddles, these are not particularly common.

To determine the resolution, tracks are found and fit as described in the previous section. One measure is to fit the line and then look at the residual for each hit to the fit line. When sufficient hits are available, it is possible to fit a track using $n-1$ of the n hits, and then look at the distance of the $n'th$ hit to resulting line. Both methods are used and compared in determining the chamber resolution.

13.4 dE/dx Studies in The CDC

In the final GlueX detector, there is a class of tracks that have transverse momentum small enough that they will be bent into circles and effectively stay within the tracking volume. One defining characteristic of these tracks is that their total momentum is less than $450\,MeV/c$. In Figure 24 we show the classic dE/dx plot reproduced from reference [15]. We do not mean to imply that the CDC will achieve this resolution, but rather to 0.2 to $0.45\,GeV/c$ region where there is a large separation between π, K and p.

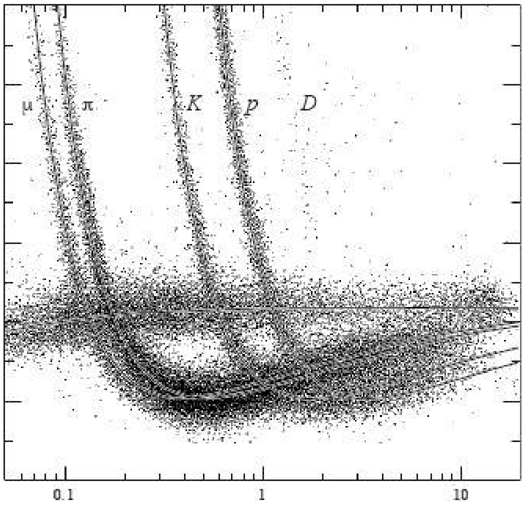

Figure 24: PEP4/9-TPC energy-deposit measurements (185 samples @8.5 atm Ar-CH4 80%20%) in multihadron events. Plot taken from the 2006 edition of the Particle Data Book.

Studies of performing dE/dx in the CDC have just started using cosmic tracks. The JETSET detector at LEAR showed that it is possible to do dE/dx measurements in a straw tube chamber [1]. Our work will follow somewhat what they did. The crucial detail that makes dE/dx in a straw different from a more conventional drift chamber is the fact that the path length of a track inside a given straw can very by large factors. This comes about both from how close to the wire the track crosses, but also the angle relative to the wire length at which the track crosses. Figure 25 shows schematically two tracks crossing through a straw tube with quite different lengths in the straw.

Our studies will use cosmic tracks that cross roughly 90° from the length

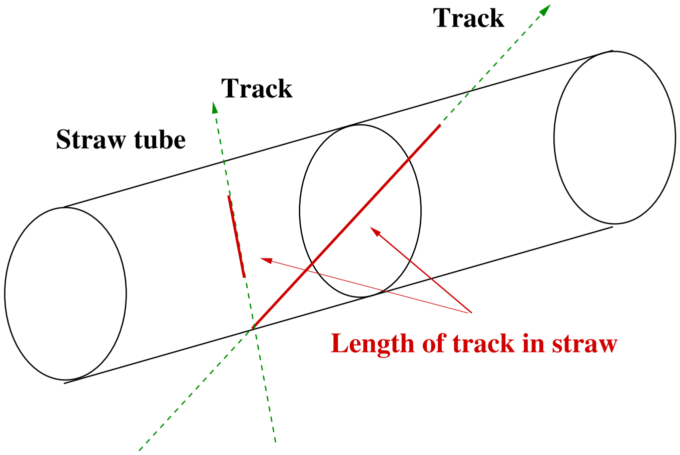

Figure 25: A schematic drawing of two tracks passing through a straw tube with quite different lengths inside the straw. In order to be able to utilize dE/dx information in the CDC, it is necessary to accurately compute the length of a track in a given straw tube.

of the wire. The track fit to several tubes will then allow us to compute the track length in a given straw tube, and thus computing the relevant dx. The energy deposit can then be computed by analytically summing the charge in a given pulse. To first order, this is simply a sum of all channels above pedestal from where the track starts until it falls back close to pedestal.

For comics, we will then assume that all particles are minimum ionizing μs, which should then produce (roughly) the same dE/dx. Looking at the spread in this for a large number of tracks will allow us to set limits on how well this measurement can be performed.

13.5 Future Activities

Given that we are still nearly a year away from the proposed start of construction of the 12 GeV upgrade, we anticipate utilizing the time to continue to study the prototype.

Over the next six to nine months, we anticipate extending this work to include tracks crossing through the chamber at a wide range of angles. We also anticipate looking at the energy-loss information for cosmics—mostly with the goal of understanding the correct track-length and angle corrections.

Finally, we anticipate investigating charge-division measurements in the chamber. This would be accomplished by connecting the down-stream ends of pairs of wires together and then studying the effective z-resolution that can be obtained. It is believe that z resolution on the order of $10\,cm$ could be obtained. This would be extremely useful in the pattern recognition step of track reconstruction in the chamber.

14 List of Design Parameters

Table 6: Geometry

Active volume inner radius:	10.18 cm
Active volume outer radius:	55.42 cm
Active length:	150 cm
Chamber assembly outer radius:	60.0 cm
Axial layers (1-3):	10.16 to 15.32 cm
Stereo layers (4-7):	15.5 to 22.45 cm
Axial layers (8-12):	23.9 to 32.63 cm
Stereo layers (13-16):	32.81 to 39.76 cm
Axial layers (17-24):	40.81 to 55.42 cm
Thickness per layer (g/cm2):	0.051
Thickness per layer (rad. lengths):	0.0014
Thickness per 24 layers (rad. lengths):	0.035

Table 7: Material

Gas (at 1 at.):	Ar/CO_2 90/10
Gas (at 1 at.):	$Ar/CO_2/CH_4$ 80/10/10 (possibly)
Number of cables : (50-conductor shielded ribbon cables)	$3098/24 = 130$
Positioning accuracy of sense wires (x,y):	$40\,\mu m$
Positioning accuracy of package (z):	$0.5\,mm$
Thickness of inner shell (g/cm2):	0.162
Thickness of inner shell (rad. lengths):	0.0067
Thickness of outer shell (g/cm2):	$1.02\,cm$ of fiberglass
Thickness of outer shell (rad. lengths):	0.031
Strawtube (diameter):	$1.6\,cm$
Strawtube (material):	Aluminized Kapton
Strawtube (thickess):	$100(5)\,\mu m$ Kapton(Al)
Number of sense wires (20 micron gold-plated W):	$3098 \pm 1.5\%$
Upstream End plate:	$0.9525\,cm$ Al (3/8 plate)
Downstream End plate:	$0.4\,cm$ Carbon Fiber
Upstream Feedthrus:	Al
Downstream Feedthrus:	Delrin
Plenums:	Plexiglas

Table 8: Location active area

Upstream gas plenum:	$-3\,cm$
Upstream active volume:	$17\,cm$
Downstream active volume:	$167\,cm$
Downstream gas plenum:	$177\,cm$

Table 9: dE/dX capability

Sense wires:	YES
Momentum Range:	$p \leq 450 MeV/c$

Table 10: Operation:

Nominal operating voltage (sense):	$+1900\,V$
Nominal gas gain:	5×10^4
Gas flow:	$5/day$

Table 11: Preamplifier and Readout

Nominal gain:	5×10^4
Noise level:	
Rise time:	$\sim 50\,ns$
Tail compensation:	YES
Cable length to post-amp:	$30\,m$
Discriminator output:	NO
Sense wires:	$125\,MHz$ FADCs

Table 12: Calibration and Resolution

Sense wires (selected charge):	electronic pulser
Perpendicular to wire (σ):	$150\,\mu m$
z-position from stereo (σ):	$2\,mm$
z-position from charge division:	$8\,cm$

References

[1] H. Wirth, *et al.* (The JETSET Collaboration), **Particle Identification with the JETSET Straw Chambers**, Nucl. Instrum. Methods A**367**, 248, (1995).

[2] The GlueX Collaboration, **The GlueX Detector Review Mini-Design-Report**, GlueX Document 346, October 2004.

[3] F. Sauli, **Principles of Operation of Mulyiwire Proportional and Drift Chambers**, CERN Report 77-09 (1977).

[4] Rob Veenhof, **The GARFIELD Program, Simulation of Gaseous Detectors**", `http://garfield.web.cern.ch/garfield/`, (1984).

[5] Zebulun Krahn and Curtis A. Meyer, **Gas Composition Study for the Straw Tube Chamber in the GlueX Detector at Jefferson Lab**, GlueX Document 62, November 2002.

[6] Curtis A. Meyer, **A Study of Vertex Resolution in GlueX**, GlueX Document 388, November 2004.

[7] Curtis A. Meyer, **The GlueX Central Drift Chamber**, GlueX Documnet 744, February 2007.

[8] gluex-764 Curtis A. Meyer, **Budget Justification for the GlueX Central Drift Chamber**, GlueX Document 764, July 2007.

[9] gluex-928Yves van Haarlem and Curtis A. Meyer, **The CDC High-voltage Board**, GlueX Document 928, December 2007.

[10] gluex-979Curtis A. Meyer and Yves van Haarlem, **The CDC Design Layout**, GlueX Document 979, February 2008.

[11] Dan Carman, **FDC On-Chamber Electronics**, GlueX-doc-753, February 2007.

[12] Fernando Barbosa, **GlueX Preamp Card User's Manual**, GlueX Document 923, December 2007.

[13] Fernando Barbosa, **Low Voltage Distribution for the Hall D CDC and FDC Detectors** GlueX Document 966, January 2008.

[14] Fernando Barbosa, **High Voltage Distribution for the Hall D CDC and FDC Detectors** GlueX Document 967, February 2008.

[15] W.-M.Yao *et al.* (Particle Data Group), J. Phys. G **33**, 1 (2006)